Contribution of J mixing to the $^5D_0$-$^7F_0$ transition of Eu^{3+} ions in several host matrices

Masanori Tanaka, Goro Nishimura,* and Takashi Kushida
Department of Physics, Osaka University, Toyonaka, Osaka 560, Japan
(Received 14 December 1993)

The $^5D_0$-$^7F_0$ transition mechanism has been investigated for the Eu^{3+} ion in two kinds of oxide glasses, polyvinyl alcohol film, and Y_2O_2S crystal powder, from the analysis of the laser-induced fluorescence spectra. In the case of Eu^{3+} in sodium silicate glass and sodium germanate glass, it has been found that the $^5D_0$-$^7F_0$ transition probability of the ions site-selected by the laser-light excitation is approximately proportional to the square of the axial second-order crystal-field parameter B_{20}. The interpretation of this result is that the dominant mechanism of this transition in these two glasses is due to the borrowing of intensity from the $^5D_0$-$^7F_2$ ($M_J=0$) transition by the J-mixing effect. In the case of polyvinyl alcohol:Eu^{3+} and Y_2O_2S:Eu^{3+}, on the other hand, the contribution of this mechanism has been found to be negligible, from the analysis of the intensity ratio between the $^5D_0$-$^7F_0$ and $^5D_0$-$^7F_2$ transitions. Furthermore, in the above two kinds of glass samples, the site-to-site variations in the energy of the $^7F_0$ state and the mean energy of the three $^7F_1$ Stark levels are explained well by the mixing of the $^7F_2$ state due to the second-order crystal-field potential. To explain the above energy variations in polyvinyl alcohol:Eu^{3+}, however, it is necessary, in addition to this effect, to take into account the mixing of the charge-transfer state and/or the J mixing due to the other components of the crystal-field potential.

I. INTRODUCTION

The electric dipole transitions within the $4f$ shell of rare-earth ions are usually explained by the Judd-Ofelt theory.[1,2] According to this theory, the $^5D_0$-$^7F_0$ transition of the Eu^{3+} ion is forbidden on account of the closure approximation employed for the high-lying states which mix into the $4f^6$ states through the odd-parity crystal-field components. Furthermore, the magnetic dipole and electric quadrupole transitions are forbidden for this line by the selection rule. Nevertheless, the $^5D_0$-$^7F_0$ transition of the Eu^{3+} ion is often observed in the materials in which the site symmetries of this ion are relatively low.[3-6] Three types of mechanisms are able to account for this transition. The first is the breakdown of the closure approximation in the Judd-Ofelt theory, which was employed for the high-lying odd-parity states to admix into the $^5D_0$ and $^7F_0$ states through the crystal-field potential. The second is based on the mechanism proposed by Wybourne[7] and subsequently developed by Downer and co-workers.[8,9] In this mechanism, the spin-selection rule is relaxed by the spin-orbit interaction acting within the high-lying odd-parity states which serve as the intermediate states of the electric dipole f-f transition. In the above two mechanisms, the $^5D_0$-$^7F_0$ transition can be caused through the linear term of the crystal-field potential.[3-6] The third is due to the mixing of the $4f^6$ states into the $^5D_0$ and $^7F_0$ states by the even-parity crystal-field perturbation.[5,7,10-12] This J-mixing effect makes it possible for the $^5D_0$-$^7F_0$ transition to borrow intensity from the $^5D_0$-^7F_J ($J=2$, 4, and 6) and ^5D_J-$^7F_0$ ($J=2$ and 4) transitions, which are explained by the Judd-Ofelt and Wybourne-Downer theories. In this mechanism, the presence of the linear term of the crystal-field potential is not necessary.

In this paper, we analyze the fluorescence spectra of Eu^{3+} in two kinds of oxide glasses, polyvinyl alcohol film and Y_2O_2S crystal powder measured with the laser-induced fluorescence line-narrowing technique. From the result, we examine which of the above three mechanisms explains the $^5D_0$-$^7F_0$ transition of the Eu^{3+} ion. In the oxide glasses and polyvinyl alcohol, the energy levels of the Eu^{3+} ion have wide distributions on account of the relatively large site-to-site variation in the crystal-field strength acting on the ion. From the relation between the $^5D_0$-$^7F_0$ and $^5D_0$-$^7F_1$ energy separations for various sites, we also examine which component of the crystal-field potential is responsible for the variations of the energies of the $^7F_0$ and $^7F_1$ states. A part of the present result has already been reported briefly.[12]

II. THEORY

In this section, we calculate the transition matrix elements for the three possible $^5D_0$-$^7F_0$ transition mechanisms mentioned above. If the electron configuration and spins of the $^5D_0$ and $^7F_0$ states are good quantum numbers, the $^5D_0$-$^7F_0$ transition is forbidden by the parity- and spin-selection rules. These selection rules are, however, relaxed by the perturbations due to the odd-parity components of the crystal-field potential acting on the Eu^{3+} ion and the spin-orbit interaction of the electrons of the ion, respectively. Thus, we adopt the Russell-Saunders states as the basis and use the second-order perturbation theory in order to take the above two perturbations into account simultaneously.

Now, we expand the crystal-field potential acting on the Eu^{3+} ion as

$$V_C=\sum_k V_C^{(k)}=\sum_{k,q,j} B_{kq}C_q^{(k)}(\theta_j,\phi_j) \quad (1)$$

with

$$C_q^{(k)}=\sqrt{4\pi/(2k+1)}Y_{kq} ,$$

where Y_{kq} is the q component of the kth-order spherical harmonics and (r_j, θ_j, ϕ_j) is the position of the jth $4f$ electron of the Eu^{3+} ion. Then, the transition matrix element of the electric dipole moment μ for the $^5D_0$-$^7F_0$ transition is expressed by the sum of two terms as follows:

$$T(^5D_0\rightarrow{}^7F_0)=\langle A\rangle+\langle B\rangle , \tag{2}$$

where

$$\langle A\rangle=\sum_{L,L'}\left\{\frac{\langle f^6\,{}^7F_0|\mu|{}^7L_1'^{\rm odd}\rangle\langle{}^7L_1'^{\rm odd}|V_C^{(1)}|f^6\,{}^7L_0^{\rm even}\rangle\langle f^6\,{}^7L_0^{\rm even}|H_{\rm SO}|f^6\,{}^5D_0\rangle}{E({}^7L_0^{\rm even}-{}^5D_0)E({}^7L_1'^{\rm odd}-{}^5D_0)}\right.$$
$$+\frac{\langle f^6\,{}^7F_0|H_{\rm SO}|f^6\,{}^5L_0^{\rm even}\rangle\langle f^6\,{}^5L_0^{\rm even}|V_c^{(1)}|{}^5L_1'^{\rm odd}\rangle\langle{}^5L_1'^{\rm odd}|\mu|f^6\,{}^5D_0\rangle}{E({}^5L_1'^{\rm odd}-{}^7F_0)E({}^5L_0^{\rm even}-{}^7F_0)}$$
$$+\frac{\langle f^6\,{}^7F_0|H_{\rm SO}|f^6\,{}^5L_0^{\rm even}\rangle\langle f^6\,{}^5L_0^{\rm even}|\mu|{}^5L_1'^{\rm odd}\rangle\langle{}^5L_1'^{\rm odd}|V_C^{(1)}|f^6\,{}^5D_0\rangle}{E({}^5L_1'^{\rm odd}-{}^5D_0)E({}^5L_0^{\rm even}-{}^7F_0)}$$
$$\left.+\frac{\langle f^6\,{}^7F_0|V_C^{(1)}|{}^7L_1'^{\rm odd}\rangle\langle{}^7L_1'^{\rm odd}|\mu|f^6\,{}^7L_0^{\rm even}\rangle\langle f^6\,{}^7L_0^{\rm even}|H_{\rm SO}|f^6\,{}^5D_0\rangle}{E({}^7L_1'^{\rm odd}-{}^7F_0)E({}^7L_0^{\rm even}-{}^5D_0)}\right\} . \tag{3}$$

and

$$\langle B\rangle=\sum_{L',L''}\left\{\frac{\langle f^6\,{}^7F_0|\mu|{}^7L_1''^{\rm odd}\rangle\langle{}^7L_1''^{\rm odd}|H_{\rm SO}|{}^5L_1'^{\rm odd}\rangle\langle{}^5L_1'^{\rm odd}|V_C^{(1)}|f^6\,{}^5D_0\rangle}{E({}^7L_1''^{\rm odd}-{}^5D_0)E({}^5L_1'^{\rm odd}-{}^5D_0)}\right.$$
$$\left.+\frac{\langle f^6\,{}^7F_0|V_C^{(1)}|{}^7L_1''^{\rm odd}\rangle\langle{}^7L_1''^{\rm odd}|H_{\rm SO}|{}^5L_1'^{\rm odd}\rangle\langle{}^5L_1'^{\rm odd}|\mu|f^6\,{}^5D_0\rangle}{E({}^7L_1''^{\rm odd}-{}^7F_0)E({}^5L_1'^{\rm odd}-{}^7F_0)}\right\} . \tag{4}$$

Here, $E(j-k)=E(j)-E(k)$ is the energy separation between the j and k states.

The spin-orbit interaction acting within the $4f^6$ configuration states relaxes the spin-selection rule in the term $\langle A\rangle$, while that within the high-lying electron configuration states does so in the term $\langle B\rangle$. Further, the linear term of the crystal-field potential plays essential roles in both of the terms $\langle A\rangle$ and $\langle B\rangle$. Qualitatively, the expressions (2)–(4) are sufficient. However, strictly speaking, the term $\langle A\rangle$ needs to be improved, because it is usually not appropriate to treat the spin-orbit interaction within the $4f^N$ configuration states as a perturbation. This is because the magnitude of the spin-orbit interaction of the $4f$ electron is comparable to that of the Coulomb interaction between the $4f$ electrons in rare-earth ions, and the energy separations between different pure Russell-Saunders states originating from the $4f^6$ electron configuration are not large enough. Therefore, the intermediate coupling approximation should be generally employed. On the other hand, it is possible to regard the spin-orbit interaction within the high-lying electron configuration states as the perturbation, because the energy separations between these states and the $4f^N$ states are very large. For the above reason, we need to revise only the term $\langle A\rangle$ into the following form:

$$\langle A'\rangle=-\sum_{SL'}\left\{\frac{\langle f^6[{}^7F]_0|\mu|{}^{2S+1}L_1'^{\rm odd}\rangle\langle{}^{2S+1}L_1'^{\rm odd}|V_C^{(1)}|f^6[{}^5D]_0\rangle}{E({}^{2S+1}L_1'^{\rm odd}-[{}^5D]_0)}\right.$$
$$\left.+\frac{\langle f^6[{}^7F]_0|V_C^{(1)}|{}^{2S+1}L_1'^{\rm odd}\rangle\langle{}^{2S+1}L_1'^{\rm odd}|\mu|f^6[{}^5D]_0\rangle}{E({}^{2S+1}L_1'^{\rm odd}-[{}^7F]_0)}\right\} . \tag{5}$$

Here, the square brackets represent that the quantities in the parentheses are not good quantum numbers on account of the intermediate coupling approximation.

The transition matrix element of the type $\langle B \rangle$ corresponds to the mechanism proposed by Wybourne[7] and developed by Downer and coworkers.[8,9] The term $\langle B \rangle$ includes two energy denominators, while the expression (5) has only one energy denominator. Therefore, the transition matrix element of the term $\langle B \rangle$ is much more sensitive than $\langle A' \rangle$ to the energy difference between the high-lying odd-parity states and the states concerned with the optical transition.

If we adopt the closure approximation for the high-lying states $|^{2S+1}L'^{\text{odd}}_1\rangle$ in the expression (5), the matrix element of the electric dipole moment μ for the $^5D_0$-$^7F_0$ transition is expressed as

$$\langle A' \rangle \propto \langle 4f^6[^7F]_0 \| U^{(0)} \| 4f^6[^5D]_0 \rangle , \quad (6)$$

where $\langle \| U^{(0)} \| \rangle$ is the reduced matrix element of the unit tensor operator $U^{(0)}$. Since $U^{(0)}$ is a constant, the matrix element (6) vanishes on account of the orthogonality of the wave functions.[7] Therefore, the Judd-Ofelt theory[1,2] predicts zero intensity for the $^5D_0$-$^7F_0$ transition. However, when we do not employ the closure approximation, this transition is allowed through the linear term of the crystal-field potential, as shown in the expression (5).

In the case of Eu^{3+}, the charge-transfer states lie at lower energies, compared with the states of the $4f^55d$ and $4f^55g$ configurations. This is because the $4f^6$ configuration of the Eu^{3+} ion is favorable to the migration of an electron from a ligand into a Eu^{3+} ion for the stability of the half-filled electron shell of the $4f^7$ configuration.[13] Furthermore, the lower levels of the charge-transfer states are septets and nonets,[14] which correspond to the states where one hole couples with the Eu^{2+} ion in the ground state ^8S. These septets admix, through $V_C^{(1)}$ in Eq. (5), into the $^7F_0$ state and also into the $^5D_0$ state, because the $^7F_0$ wave function is mixed into the latter state considerably by the spin-orbit interaction within the $4f^6$ configuration states. (This admixture of the charge-transfer state was called the spin-restricted covalency effect by Hoshina, Imanaga, and Yokono.[14]) Thus, in the $^5D_0$-$^7F_0$ transition mechanism of the term $\langle A' \rangle$, the septet charge-transfer state is considered to play the dominant role as the high-lying odd-parity states which admix into the $4f^6$ states.[6,14-16] If the energy of this charge-transfer state is so low that the closure approximation breaks down, the $^5D_0$-$^7F_0$ electric dipole transition arises by the mixing of this charge-transfer state into the $^7F_0$ and $^5D_0$ states in the mechanism of the expression (5). In the mechanism of the term $\langle B \rangle$, on the other hand, the $4f^55d$ electron configuration state and the quintet charge-transfer state are considered to be important as the $^5L'^{\text{odd}}_1$ state in the expression (4). The probable quintet charge-transfer state is the state in which one hole is trapped by the Eu^{2+} ion in the excited state ^6L (L is the total angular momentum of the Eu^{2+} ion). The energy of this state is considered to be much higher than the septet charge-transfer state and possibly than the $4f^55d$ states. Thus, the $4f^55d$ states may be more effective than the charge-transfer states as the high-lying odd-parity states in expression (4). In the case of Sm^{2+}-doped glass, the $^5D_0$-$^7F_0$ transition strength is much larger than that in Eu^{3+}-doped glass.[17] In Sm^{2+}, the $4f^55d$ states are much closer in energy to the $4f^6$ configuration states, and the contribution of the term $\langle B \rangle$ is considered to be much larger than in Eu^{3+}. This will explain the large difference in the $^5D_0$-$^7F_0$ transition strength in Sm^{2+} and Eu^{3+} glasses.

There exists another mechanism of the $^5D_0$-$^7F_0$ transition due to the J-mixing effect.[5,7,10-12] Because the ^7F_J ($J=2$, 4, and 6) and ^5D_J ($J=2$ and 4) states admix into the $^7F_0$ and $^5D_0$ states by the even-parity crystal-field perturbation, the $^5D_0$-$^7F_0$ transition can obtain intensities from the transitions between the ^5D_J ($J=2$ and 4) and $^7F_0$ states or between the $^5D_0$ and ^7F_J ($J=2$, 4, and 6) states, which are explained by the Judd-Ofelt and Wybourne-Downer theories. The dominant contribution may come from the admixture of the $^7F_2$ state into the $^7F_0$ state, because the $^7F_2$-$^7F_0$ energy separation is the smallest in all the energy separations between the $^7F_0$ and $^5D_0$ states and the $4f^6$ states that mix into them, and also because the fluorescence due to the $^5D_0$-$^7F_2$ transition is more intense compared with those due to the $^5D_0$-$^7F_4$ and $^5D_0$-$^7F_6$ transitions in our samples. When we take into account the energy denominators and the magnitude of the reduced matrix element in the J-mixing coefficients, the J-mixing effect for the $^5D_0$ state is found to be much smaller than that for the $^7F_0$ state. Thus, we consider only the mixing of $^7F_2$ into $^7F_0$. Then, we can express the wave function of the $^7F_0$ state as

$$|f^6[^7F_0]\rangle = |f^6[^7F]_0\rangle - \frac{2\sqrt{3}}{15\Delta_{20}} \sum_{q=-2}^{2} (-1)^q B_{2q} \times |f^6[^7F]_2 M_J = q\rangle , \quad (7)$$

where $\Delta_{JJ'}$ is the energy separation between the ^7F_J and $^7F_{J'}$ states at the free ion state. Here, we made a calculation by regarding the $^7F_0$ and $^7F_2$ states in a free ion state as pure Russell-Saunders states, because, according to Ofelt,[18] the L-S coupling holds fairly well for the ^7F_J states of the Eu^{3+} ion. Then, the transition matrix element of the $^5D_0$-$^7F_0$ transition is expressed, using Eqs. (2) and (7), as

$$\langle [f^6\,^5F_0]|\mu|[f^6\,^7D_0]\rangle = T(^5D_0 \rightarrow {}^7F_0) - \frac{2\sqrt{3}}{15\Delta_{20}} \sum_{q=-2}^{2} (-1)^q B_{2-q} \times T(^5D_0 \rightarrow {}^7F_2 M_J = q\rangle . \quad (8)$$

Here, $T(^5D_0 \rightarrow {}^7F_J M_J)$ denotes the sum of the transition matrix element for the $^5D_0$-$^7F_J(M_J)$ transition in the Judd-Ofelt theory[1,2] and that in the Wybourne-Downer theory.[8,9] The second term of Eq. (8) corresponds to the effect of the J mixing, and shows that the $^5D_0$-$^7F_0$ transition obtains intensity from the $^5D_0$-$^7F_2$ transition.

We have examined which of the above three mechanisms makes the dominant contribution to the $^5D_0$-$^7F_0$ transition in several matrices, and also investigated the mechanism of the inhomogeneous broadening of the spectral lines.

III. EXPERIMENTAL RESULTS AND DISCUSSION

A. The $^5D_0$-$^7F_0$ transition mechanism

1. *Eu^{3+}-doped sodium silicate and sodium germanate glasses*

The fluorescence spectra were measured for Eu^{3+}-doped sodium silicate glass [(1) Eu_2O_3·(30) Na_2O·(70)SiO_2 (mole) ratio] and sodium germanate glass [(1) Eu_2O_3·(20)Na_2O·(80)GeO_2] at 77 K under the site-selective $^7F_0$-$^5D_0$ and $^7F_1$-$^5D_0$ excitations with a cw rhodamine-6G dye laser. Figure 1 shows the fluorescence spectra due to the $^5D_0$-^7F_J ($J=0$ and 1) transitions under the excitation from the lowest level of the three Stark levels of $^7F_1$ to the $^5D_0$ state in the Eu^{3+}-doped sodium silicate glass. The $^5D_0$-$^7F_0$ line shifts to the higher energies with the increase of the $^7F_1$-$^5D_0$ excitation energy. A similar result was obtained also for the Eu^{3+}-doped sodium germanate glass. From the presence of the $^5D_0$-$^7F_0$ transition and the splitting of the $^7F_1$ manifold into three levels, the symmetry of the Eu^{3+} ion site in these samples is found to be C_{2V}, C_2, C_S, or C_1. In the sodium germanate glass, six fluorescence lines were observed in the region of the $^5D_0$-$^7F_2$ transition. This result shows that the plural kinds of sites exist in this sample. However, the $^5D_0$-$^7F_0$ and the three $^5D_0$-$^7F_1$ fluorescence lines shift continuously with changing the $^7F_1$-$^5D_0$ and $^7F_0$-$^5D_0$ excitation energies. Therefore, we consider that one kind of site exists dominantly, and accordingly hereafter we neglect the contribution of the minor kinds of sites to the fluorescence spectra. In the sodium silicate glass, five $^5D_0$-$^7F_2$ transition lines were observed, and the $^5D_0$-$^7F_0$ and $^5D_0$-$^7F_1$ fluorescence lines again shifted continuously with the $^7F_1$-$^5D_0$ and $^7F_0$-$^5D_0$ excitation energies. If these lines originate from one kind of site, the point symmetry C_{2V} must be excluded, because only four electric dipole $^5D_0$-$^7F_2$ transition lines are allowed in this symmetry.

As shown in Fig. 2, with increasing excitation energy within the inhomogeneously broadened $^7F_0$-$^5D_0$ absorption band, the highest-energy line among the three $^5D_0$-$^7F_1$ lines shifts remarkably to the higher energies in sodium silicate glass, while the energy positions of the other two lines do not vary much. This property was also observed for the sodium germanate glass. In addition, it is known that other kinds of oxide glasses also exhibit similar properties.[19] This behavior is ascribed to the difference of the symmetries of the wave functions describing the three $^7F_1$ Stark levels. In C_{2V}, C_2, and C_S symmetries, the $M_J=0$ component (ϵ_0) of the $^7F_1$ Stark levels has a large electron distribution in the z axis, while the other components ($\epsilon_\pm$) along the x-y plane. In C_1 symmetry, there is not much difference in the symmetries of the three wave functions. Therefore, the site symmetry of the Eu^{3+} ion is considered to be restricted to C_{2V}, C_2, and C_S, and the lowest one in the $^7F_1$ Stark levels can be assigned to the $M_J=0$ component in each site symmetry. Previously, a quite similar shift of the three $^5D_0$-$^7F_1$ lines was observed in Eu^{3+}-doped Ca $(PO_3)_2$ glass, and the above assignment was verified by the polarization correlation between the $^7F_0$-$^5D_0$ excitation and $^5D_0$-$^7F_1$

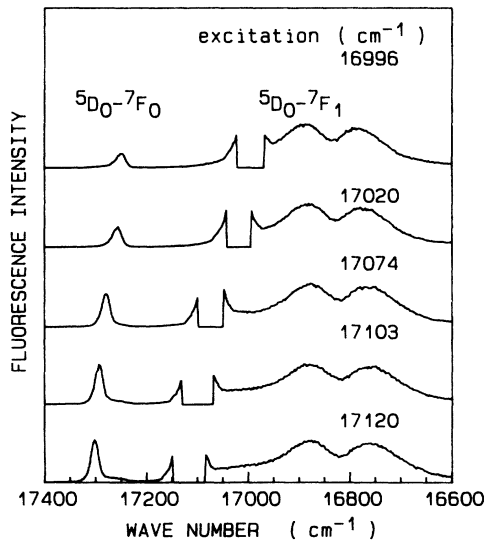

FIG. 1. Fluorescence spectra of sodium silicate glass doped with Eu^{3+} at 77 K under the laser excitation from the lowest level of the $^7F_1$ state to the $^5D_0$ state. The fluorescence intensity is normalized to the peak value of the lowest-energy line of the $^5D_0$-$^7F_1$ transition.

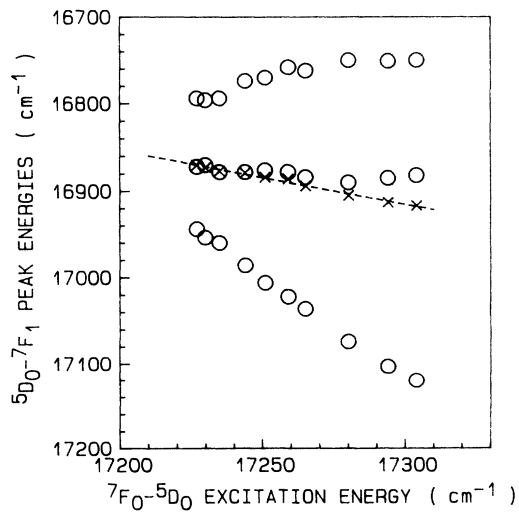

FIG. 2. Peak energies (circles) and the mean energy (crosses) of the three $^5D_0$-$^7F_1$ fluorescence lines in sodium silicate glass doped with Eu^{3+} at 77 K plotted as a function of the $^7F_0$-$^5D_0$ excitation energy. The dashed straight line is fitted for the above mean energy by the least-squares method, and has a slope of 0.62. The linear correlation coefficient is 0.99 for this fitting.

fluorescence.[20] By this assignment, the values of the second-order crystal-field parameters B_{20} and $|B_{2\pm2}|$ were determined for the sites selected by the $^7F_0$-$^5D_0$ excitation, from the energy separations among the three $^5D_0$-$^7F_1$ fluorescence lines. We considered only the mixing within the $^7F_1$ manifold, and used the following expressions for the energies of the three Stark levels of the $^7F_1$ manifold:

$$E(\epsilon_0)=E_0(^7F_1)+\frac{B_{20}}{5}\ , \tag{9a}$$

$$E(\epsilon_\pm)=E_0(^7F_1)-\frac{B_{20}}{10}\pm\frac{\sqrt{6}|B_{2\pm2}|}{10}\ , \tag{9b}$$

where $E_0(^7F_1)$ is the energy of the $^7F_1$ state when the second-order crystal-field component $V_C^{(2)}$ is zero. Then, it was found that the value of the axial crystal-field parameter B_{20} varies markedly with the $^7F_0$-$^5D_0$ excitation energy, while that of $|B_{2\pm2}|$, which indicates the strength of the x-y component of the second-order crystal field, does not vary much.

The $^5D_0$-$^7F_1$ transition is the parity-allowed magnetic dipole transition and its strength hardly varies with the crystal-field strength acting on the Eu^{3+} ion. For this reason, the intensity ratios of the $^5D_0$-$^7F_0$ and $^5D_0$-$^7F_2$ transitions to the $^5D_0$-$^7F_1$ transition under a site-selective excitation are considered to be good measures of the $^5D_0$-$^7F_0$ and $^5D_0$-$^7F_2$ transition strengths for the ions in the selected site. Figure 3 shows these intensity ratios as a function of B_{20}^2 in the Eu^{3+}-doped sodium silicate glass. In this figure, we notice the following: (I) The $^5D_0$-$^7F_0$ transition strength is nearly proportional to B_{20}^2, (II) the $^5D_0$-$^7F_2$ transition strength is independent of the variation of B_{20}^2.

The same results were also obtained for the Eu^{3+} ion in sodium germanate glass and previously for the Eu^{3+}-doped $Ca(PO_3)_2$ glass.[11,12] If we try to explain these results by the $^5D_0$-$^7F_0$ transition mechanism due to the breakdown of the closure approximation and/or Wybourne and Downer's mechanism, it is necessary that the linear term of the crystal-field potential varies in proportion to the value of B_{20}^2. However, it is not probable that this proportionality holds accidentally in various glasses. On the contrary, we can interpret the above experimental results well by the second term of Eq. (8), i.e., by the mechanism that the $^5D_0$-$^7F_0$ transition borrows intensity from the $^5D_0$-$^7F_2$ ($M_J=0$) transition through the J mixing due to the axial second-order crystal-field component $B_{20}C_0^{(2)}$. The electric dipole $^5D_0$-$^7F_2$ ($M_J=0$) transition arises through the Judd-Ofelt and Wybourne-Downer mechanisms when one of the crystal-field parameters B_{10}, $B_{1\pm1}$, B_{30}, and $B_{3\pm1}$ is present. Some of these crystal-field parameters are certainly present in the point symmetries C_{2V}, C_2, or C_S of the Eu site.

When the J-mixing effect through $B_{20}C_0^{(2)}$ makes a dominant contribution to the $^5D_0$-$^7F_0$ transition, the fluorescence intensity ratio of this transition to the $^5D_0$-$^7F_2$ transition is approximately given by

$$\frac{I(^5D_0\text{-}^7F_0)}{I(^5D_0\text{-}^7F_2)}=\frac{4B_{20}^2}{375\Delta_{20}^2}\left[\frac{E(^5D_0\text{-}^7F_0)}{E(^5D_0\text{-}^7F_2)}\right]^3\ , \tag{10}$$

where $E(^5D_0\text{-}^7F_J)$ is the energy of the $^5D_0$-^7F_J transition.[11] Here, we have assumed that the transition strength of the $^5D_0$-$^7F_2$ ($M_J=0$) line is 1/5 of the total $^5D_0$-$^7F_2$ transition strength. For the site of $E(^5D_0\text{-}^7F_0)=17\,280\ cm^{-1}$ in sodium germanate glass and sodium silicate glass, the intensity ratio of Eq. (10) is calculated to be 0.01 and 0.008, respectively, using $\Delta_{20}=1036\ cm^{-1}$.[17] These values are of the same order of magnitude as the experimental values of 0.017 and 0.016 obtained for the above respective samples. Therefore, we conclude that the mixture of the $^7F_2$ ($M_J=0$) state into the $^7F_0$ state plays a dominant role in the intensity of the $^5D_0$-$^7F_0$ fluorescence in these two glass materials.

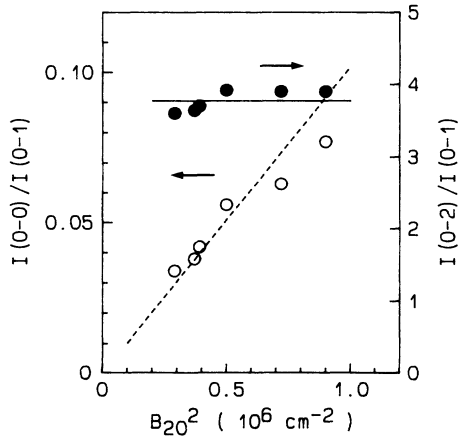

FIG. 3. Intensity ratios of the $^5D_0$-$^7F_0$ (open circles) and $^5D_0$-$^7F_2$ (closed circles) transitions to the $^5D_0$-$^7F_1$ transition for sodium silicate glass doped with Eu^{3+} ions at 77 K as a function of B_{20}^2.

2. *Eu^{3+}-doped polyvinyl alcohol film*

Figure 4 shows the fluorescence spectrum of a polyvinyl alcohol film containing $Eu(NO_3)_3\cdot6H_2O$. Similarly as in sodium germanate and sodium silicate glasses, the fluorescence intensity of the $^5D_0$-$^7F_2$ transition is larger than those of the $^5D_0$-$^7F_4$ and $^5D_0$-$^7F_6$ transitions. The fluorescence spectrum was also measured under a broad-band UV light excitation.[12] From this spectrum, it was found that the inhomogeneous widths of the fluorescence spectra due to the $^5D_0$-$^7F_0$, $^7F_1$, and $^7F_2$ transitions are narrow in this sample, compared with those in sodium germanate and sodium silicate glasses. This observation is consistent with that in a polyvinyl alcohol film containing $EuCl_3\cdot6H_2O$, which was reported by van den Berg and Völker.[21] For example, the full width at half maximum of the spectrum due to the $^5D_0$-$^7F_0$ transition in polyvinyl alcohol film was 25 cm^{-1} at 77 K, while those in sodium germanate glass and sodium silicate glass were about 100 and 70 cm^{-1} at 77 K, respectively.

As shown in Figs. 5 and 6, the fluorescence line-narrowing effect was also observed for the $^5D_0$-$^7F_1$ fluorescence lines of polyvinyl alcohol:Eu^{3+} at 77 K un-

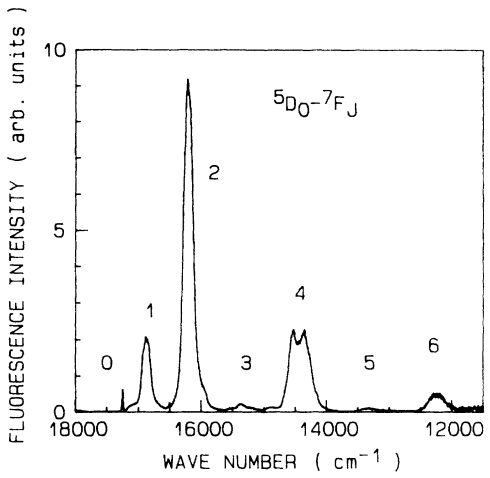

FIG. 4. Fluorescence spectrum due to the $^5D_0$-^7F_J transitions for a Eu^{3+}-doped polyvinyl alcohol film under the excitation of a 465.8-nm line of an Ar^+ ion laser at room temperature. The numbers in the figure are the inner quantum numbers J of the final states of the transitions.

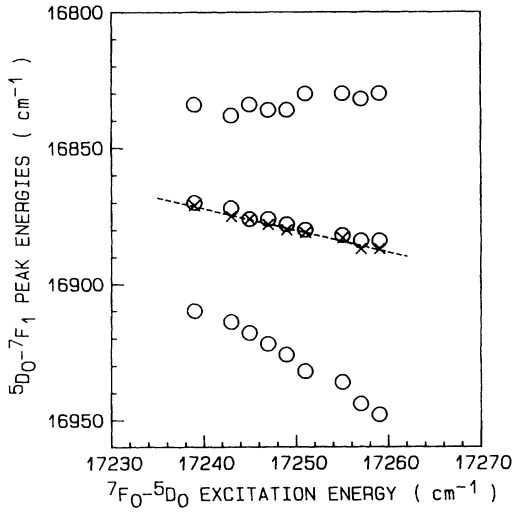

FIG. 6. Peak energies (circles) and the mean energy (crosses) of the three $^5D_0$-$^7F_1$ lines for polyvinyl alcohol:Eu^{3+} at 77 K as a function of the $^7F_0$-$^5D_0$ excitation energy. The dashed straight line is fitted for the above mean energy by the least-squares methods, and has a slope of 0.80. The linear correlation coefficient is 0.99 for this fitting.

der dye-laser excitation into the $^7F_0$-$^5D_0$ line. The highest-energy line shifts markedly to the higher energies as the $^7F_0$-$^5D_0$ excitation energy is increased. On the other hand, the other two lines do not shift very much. This situation is quite similar to those in the above two kinds of glasses. Therefore, we assign the $M_J=0$ component again to the lowest component of the $^7F_1$ Stark levels of Eu^{3+} in polyvinyl alcohol film, assuming that the point symmetry of the Eu site is C_{2V}, C_2, or C_S.

Figure 7 shows the second-order crystal-field parameters determined for the sites of various $^7F_0$-$^5D_0$ energies using this assignment. The axial crystal-field parameter B_{20} varies markedly, compared with $|B_{2\pm2}|$, with the variation of the $^7F_0$-$^5D_0$ energy. This is the same property that was observed for the two kinds of glasses treated above. For the site of $E(^5D_0$-$^7F_0)=17\,255$ cm^{-1} in polyvinyl alcohol:Eu^{3+}, where $B_{20}=-267$ cm^{-1} and

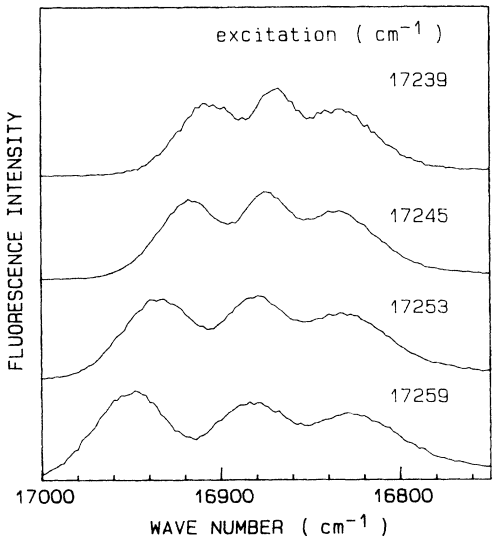

FIG. 5. Fluorescence spectra due to the $^5D_0$-$^7F_1$ transition of polyvinyl alcohol:Eu^{3+} at 77 K for various excitation energies in the $^7F_0$-$^5D_0$ absorption band.

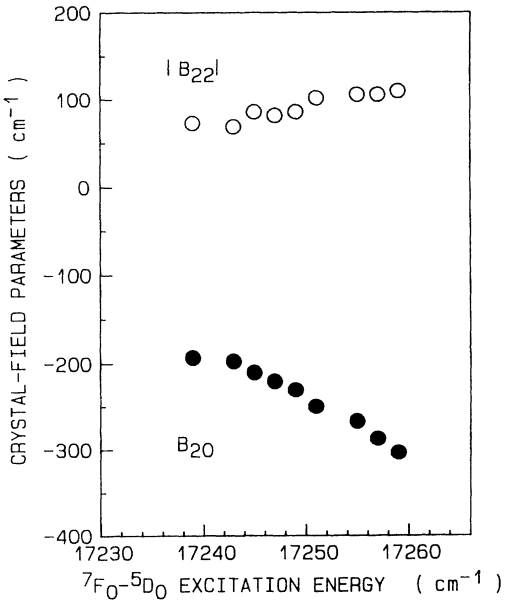

FIG. 7. Second-order crystal-field parameters in polyvinyl alcohol:Eu^{3+} as a function of the $^7F_0$-$^5D_0$ excitation energy for the site selection.

$E(^5D_0$-$^7F_2)=16\,210\ cm^{-1}$, the expression (10) is estimated as 8×10^{-4}. From the fluorescence spectrum under the $^7F_1$-$^5D_0$ excitation, the intensity ratio of the $^5D_0$-$^7F_0$ transition to the $^5D_0$-$^7F_2$ transition is obtained as 0.01. Thus, the contribution of the J mixing through the $B_{20}C_0^{(2)}$ component to the $^5D_0$-$^7F_0$ fluorescence intensity is considered to be only a small part in this sample. Furthermore, because $|B_{2\pm2}|$ is smaller than $|B_{20}|$, it is difficult to account for the intensity of the $^5D_0$-$^7F_0$ transition even if we take into account the J-mixing effect through the $B_{2\pm2}C_{\pm2}^{(2)}$ components as well as that through $B_{20}C_0^{(2)}$. Thus, in this material, the $^5D_0$-$^7F_0$ line is considered to be due to the breakdown of the closure approximation in the Judd-Ofelt theory[1,2] and/or due to Wybourne-Downer's mechanism.[8,9] As for the J-mixing effect through the fourth- and sixth-order components of the crystal-field potential, we could not examine the contribution quantitatively, because it was not possible to determine the values of the crystal-field parameters concerned from the site-selected fluorescence spectrum on account of the overlap of the fluorescence lines. However, this contribution is considered to be small.

3. *Eu^{3+}-doped Y_2O_2S crystal*

We also examined the $^5D_0$-$^7F_0$ transition mechanism in Y_2O_2S crystal which contains 5 wt. % of Eu_2O_3. Hydrostatic pressure was applied to this crystal by use of a diamond anvil cell at room temperature. The pressure was estimated from the peak shift of the R_1 line of ruby, which was put in the diamond anvil cell with Y_2O_2S:Eu^{3+}. As a result, the $^5D_0$-$^7F_0$ fluorescence line and the two lines due to the $^5D_0$-$^7F_1$ transition shifted continuously to lower energies with increasing pressure under the excitation by the 476.5-nm line of an Ar^+ laser (Fig. 8). The point symmetry of the Eu^{3+} ion site in this crystal is C_{3V}, and accordingly $|B_{2\pm2}|$ is zero. Further, it is known that the lower-energy one of the two fluorescence lines of the $^5D_0$-$^7F_1$ transition corresponds to the transition in which the $M_J=0$ component of the $^7F_1$ is the final state.[22] Therefore, we can determine the value of B_{20} for various pressures. The result is shown in Fig. 9. It is found that the value of B_{20} decreases linearly with increasing pressure. This result is qualitatively consistent with that measured by Liu, Chi, and Wang.[23]

Figure 10 shows the intensity ratios of the $^5D_0$-$^7F_0$ and $^5D_0$-$^7F_2$ transitions to the $^5D_0$-$^7F_1$ lines plotted as a function of B_{20}. The intensity ratios were estimated from the fluorescence spectra for which the wavelength dependence of the transmittance of the monochromator and the sensitivity of the photodetector was corrected, though the uncorrected spectra were used in Fig. 5 of Ref. 12. Both intensity ratios are almost constant for the variation of B_{20}. Accordingly, the mixture of the $^7F_2$ state into $^7F_0$ is not considered to make an important contribution to the $^5D_0$-$^7F_0$ fluorescence intensity in Y_2O_2S:Eu^{3+}. This is supported by the analysis of the intensity ratio of the $^5D_0$-$^7F_0$ transition to the $^5D_0$-$^7F_2$ transition, because this intensity ratio estimated from the fluorescence spectrum at 77 K is 0.01, and we find that the fraction by which the mixture of the $^7F_2$ state into the $^7F_0$ state contributes to the $^5D_0$-$^7F_0$ fluorescence intensity is only about 8 percent of the observed value, using $B_{20}=124\ cm^{-1}$ determined by Sovers and Yoshioka.[22]

Next, we consider the mixing of the $^7F_4$ state into the $^7F_0$ state, which is caused by the fourth-order crystal-field potential. Then, the wave function of the $^7F_0$ state is expressed by the perturbation calculation, as

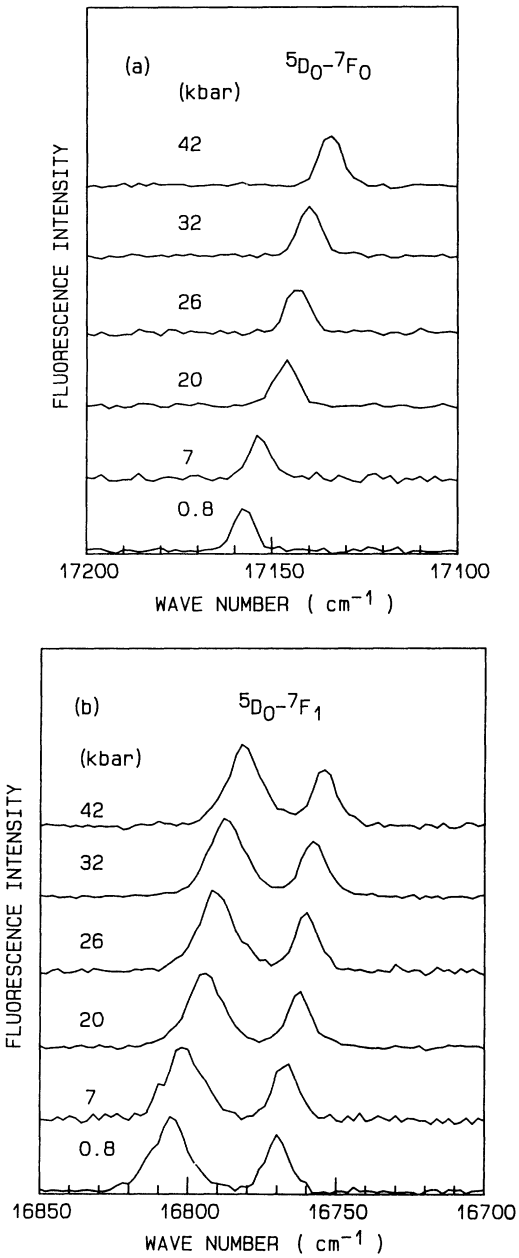

FIG. 8. Fluorescence spectra of (a) the $^5D_0$-$^7F_0$ and (b) $^5D_0$-$^7F_1$ transitions in Y_2O_2S:Eu^{3+} crystal powder under various pressures at room temperature. The excitation was done by the 476.5-nm line of an Ar^+ laser. The fluorescence intensity is normalized to the sum of the intensities of the two fluorescence lines due to the $^5D_0$-$^7F_1$ transition.

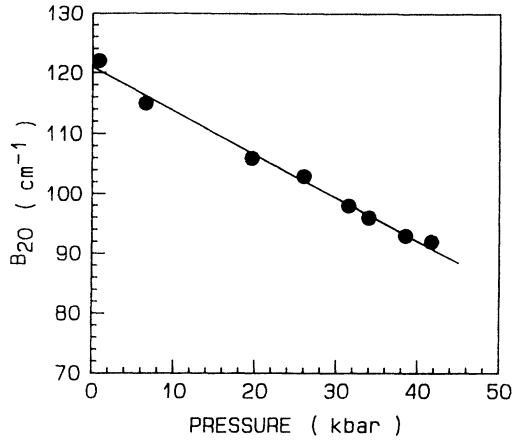

FIG. 9. Second-order axial crystal-field parameter B_{20} as a function of pressure in $Y_2O_2S:Eu^{3+}$ at room temperature.

$$|4f^6[^7F_0]\rangle = |4f^6[^7F]_0\rangle - \frac{2\sqrt{3}B_{20}}{15\Delta_{20}}|4f^6[^7F]_2 M_J=0\rangle - \frac{\sqrt{22}}{33\Delta_{40}}\sum_{q=-4}^{4}(-1)^{q+1} \times B_{4q}|4f^6[^7F]_4 M_J=q\rangle \ . \tag{11}$$

In this expression, $B_{4\pm1}$, $B_{4\pm2}$, and $B_{4\pm4}$ are zero, because the point symmetry of the Eu site in Y_2O_2S is C_{3V}. If the dominant mechanism of the $^5D_0$-$^7F_0$ transition is due to the mixing of the $^7F_4$ state into $^7F_0$, the intensity ratio of this line to the $^5D_0$-$^7F_4$ lines will be approximately given by

$$\frac{I(^5D_0\text{-}^7F_0)}{I(^5D_0\text{-}^7F_4)} = \frac{2(B_{40}^2+2B_{4\pm3}^2)}{891\Delta_{40}^2}\left[\frac{E(^5D_0\text{-}^7F_0)}{E(^5D_0\text{-}^7F_4)}\right]^3 . \tag{12}$$

Here, we have employed the assumption that the transition strengths of both the $^5D_0$-$^7F_4$ ($M_J=0$) and $^5D_0$-$^7F_4$ ($M_J=\pm3$) lines are 1/9 of the total $^5D_0$-$^7F_4$ transition strength. Employing the calculated values[22] of $B_{40}=1344\ cm^{-1}$ and $B_{4\pm3}=823\ cm^{-1}$, we find that the mixture of the $^7F_4$ state into $^7F_0$ can make a contribution of only about 5 percent to the intensity of the $^5D_0$-$^7F_0$ transition. Moreover, the contribution of the mixture of the $^7F_6$ state into $^7F_0$ through the sixth-order crystal-field component and also that of the $^5D_2$ and $^5D_4$ states into $^5D_0$ through the second- and fourth-order components, respectively, are expected to be smaller, if we take the energy separations into account. Thus, the breakdown of the closure approximation and/or Wybourne-Downer's mechanism is considered to contribute dominantly to the $^5D_0$-$^7F_0$ line in the case of $Y_2O_2S:Eu^{3+}$.

In this crystal, four oxygens are located at one side around the Eu^{3+} ion and three sulfurs at the other side.[22] This coordination, which is very different between the two sides around Eu^{3+} ion, may cause the presence of the relatively large linear term of the crystal-field potential.[4] Furthermore, the energy of the charge-transfer state involving the sulfur atom is low, compared with that involving the oxygen, on account of the relatively small electronegativity of the sulfur atom.[24] Therefore, the closure approximation is not considered to be so good for this crystal as in the two kinds of oxide glasses mentioned above, in which the Eu^{3+} ions are surrounded only by oxygens in the nearest-neighbor environment of the ion.

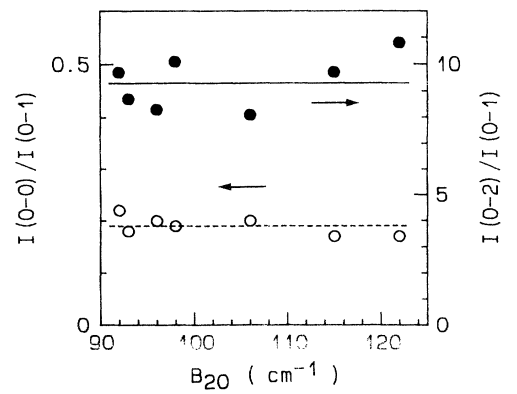

FIG. 10. Intensity ratios of the $^5D_0$-$^7F_0$ (open circles) and $^5D_0$-$^7F_2$ (closed circles) transitions to the $^5D_0$-$^7F_1$ transition as a function of B_{20} in $Y_2O_2S:Eu^{3+}$ at room temperature.

B. Relation between the energies of the $^7F_0$ state and the barycenter of the $^7F_1$ Stark levels

As mentioned before, the J-mixing effect is very small for the $^5D_0$ state compared with the ^7F_J states. Therefore, the energy distribution of the $^5D_0$ state due to the variation in the strength of the even-parity components of the crystal-field potential is much narrower than that for the ^7F_J states. When we take into consideration the J mixing in the $^7F_0$ and $^7F_1$ states only through $V_C^{(2)}$, the energy of the $^7F_0$ state and the mean energy of the three Stark levels of $^7F_1$ are expressed,[10,11] respectively, as

$$E([^7F_0]) = E_0(^7F_0) - \frac{4}{75\Delta_{20}}(B_{20}^2+2|B_{2\pm2}|^2) , \tag{13}$$

$$E_G = E_0(^7F_1) - \left[\frac{2}{75\Delta_{31}}+\frac{1}{150\Delta_{21}}\right](B_{20}^2+2|B_{2\pm2}|^2) . \tag{14}$$

From these two expressions, we predict that the energy separation between the $^5D_0$ state and the barycenter of the $^7F_1$ manifold, $E(^5D_0\text{-}E_G)$, is correlated linearly with that between the $^5D_0$ and $^7F_0$ states, $E(^5D_0\text{-}^7F_0)$. In fact, the mean energy of the three fluorescence lines due to the $^5D_0$-$^7F_1$ transition varies linearly, in the Eu^{3+}-doped sodium silicate and sodium germanate glasses, with the slope of 0.6 with the increase of the energy of the exciting $^7F_0$-$^5D_0$ light for the site-selection (for the Eu^{3+}-doped sodium silicate glass, see Fig. 2). This slope is in good

agreement with the theoretical value obtained from Eqs. (13) and (14):

$$\frac{\Delta_{20}}{8}\left[\frac{4}{\Delta_{31}}+\frac{1}{\Delta_{21}}\right]=0.54 .$$

Here, we used $\Delta_{20}=1036\ \mathrm{cm}^{-1}$, $\Delta_{31}=1524\ \mathrm{cm}^{-1}$, and $\Delta_{21}=662\ \mathrm{cm}^{-1}$, which were calculated by Ofelt.[18] In the case of polyvinyl alcohol film, the linear correlation relation was again observed between $E(^5D_0$-$E_G)$ and $E(^5D_0$-$^7F_0)$, as shown in Fig. 6. However, the slope is 0.8 and the deviation from the above-calculated value is relatively large. Therefore, we cannot ignore the contribution of the J-mixing effect due to the fourth- and sixth-order crystal-field components and/or the spin-restricted covalency effect[14] to the site-to-site variation of the energies of $^7F_0$ and $^7F_1$ in this sample.

IV. CONCLUDING REMARKS

The $^5D_0$-$^7F_0$ transition of the Eu^{3+} ion in sodium silicate and sodium germanate glasses has been shown to be caused by the mixture of the $M_J=0$ component of the $^7F_2$ manifold into the $^7F_0$ state through the second-order term of the crystal-field potential, from the analysis of the fluorescence spectra measured with the laser-induced fluorescence line-narrowing technique. On the other hand, it has been found that this transition in polyvinyl alcohol:Eu^{3+} and Y_2O_2S:Eu^{3+} cannot be explained by the above mechanism. In these samples, the breakdown of the closure approximation employed in the Judd-Ofelt theory or Wybourne-Downer's mechanism is considered to be the dominant mechanism of the $^5D_0$-$^7F_0$ transition. There exists a linear relation between the $^7F_0$-$^5D_0$ excitation energy and the mean energy of the three fluorescence lines of the $^5D_0$-$^7F_1$ transition of the Eu^{3+} ion in sodium silicate glass, sodium germanate glass, and polyvinyl alcohol film. In the former two samples, this linear relation has been explained well by the mixing of $^7F_2$ into the $^7F_0$ and $^7F_1$ states through the second-order crystal-field potential, while it has been found necessary, in polyvinyl alcohol:Eu^{3+}, to take into account the mixture of the charge-transfer state or the J-mixing effect through the fourth- and sixth-order crystal-field components, as well as the J mixing through the second-order component.

ACKNOWLEDGMENTS

The authors are indebted to Dr. S. Todoroki of NTT Corporation and Dr. M. Tamatani of Toshiba Corporation for providing us with the Eu^{3+}-doped sodium silicate and sodium germanate glasses and Y_2O_2S:Eu^{3+} powder used in this study. They are also grateful to Dr. A. Kurita for stimulating discussions.

*Present address: Research Institute for Electronic Science, Hokkaido University, Sapporo 060, Japan.

[1]B. R. Judd, Phys. Rev. **127**, 750 (1962).
[2]G. S. Ofelt, J. Chem. Phys. **37**, 511 (1962).
[3]W. C. Nieuwproort and G. Blasse, Solid State Commun. **4**, 227 (1966).
[4]G. Blasse and A. Bril, Philips Res. Rep. **21**, 368 (1966).
[5]W. C. Nieuwpoort, G. Blasse, and A. Bril, in *Optical Properties of Ions in Crystals,* edited by H. M. Crosswhite and H. W. Moos (Interscience, New York, 1967), p. 161.
[6]L. S. Gaigerova, O. F. Dudnik, V. F. Zolin, and V. A. Kudryashova, in *Luminescence of Crystals, Molecules, and Solutions,* edited by F. Williams (Plenum, New York, 1973), p. 514.
[7]B. G. Wybourne, in *Optical Properties of Ions in Crystals* (Ref. 5), p. 35.
[8]M. C. Downer, G. W. Burdick, and D. K. Sardar, J. Chem. Phys. **89**, 1787 (1988).
[9]G. W. Burdick, M. C. Downer, and D. K. Sardar, J. Chem. Phys. **91**, 1511 (1989).
[10]G. Nishimura and T. Kushida, Phys. Rev. B **37**, 9075 (1988).
[11]G. Nishimura and T. Kushida, J. Phys. Soc. Jpn. **60**, 683 (1991).
[12]G. Nishimura, M. Tanaka, A. Kurita, and T. Kushida, J. Lumin. **48/49**, 473 (1991).
[13]C. K. Jørgensen, R. Pappalardo, and E. Rittershans, Z. Naturforsch. Teil A **20**, 54 (1964).
[14]T. Hoshina, S. Imanaga, and S. Yokono, J. Lumin. **15**, 455 (1977).
[15]G. Blasse and A. Bril, Philips Res. Rep. **22**, 481 (1967).
[16]G. Blasse and A. Bril, J. Chem. Phys. **50**, 2974 (1969).
[17]M. Tanaka and T. Kushida, Phys. Rev. B **49**, 5192 (1994).
[18]G. S. Ofelt, J. Chem. Phys. **38**, 2171 (1963).
[19]M. J. Weber, in *Laser Spectroscopy of Solids,* edited by W. M. Yen and P. M. Selzer (Springer-Verlag, Berlin, 1981), p. 189.
[20]T. Kushida, E. Takushi, and Y. Oka, J. Lumin. **12/13**, 723 (1976).
[21]R. van den Berg and S. Völker, Chem. Phys. Lett. **150**, 491 (1988).
[22]O. J. Sovers and T. Yoshioka, J. Chem. Phys. **49**, 4945 (1968).
[23]S. Liu, Y. Chi, and L. Wang, J. Lumin **40/41**, 395 (1988).
[24]H. Yamamoto, Y. Otomo, and T. Kano, J. Phys. Soc. Jpn. **26**, 137 (1968).